

# Modular Deep Q Networks for Sim-to-real Transfer of Visuo-motor Policies

Fangyi Zhang, Jürgen Leitner, Michael Milford, Peter I. Corke

Australian Centre for Robotic Vision (ACRV), Queensland University of Technology (QUT)  
Brisbane, Australia  
fangyi.zhang@hdr.qut.edu.au

## Abstract:

While deep learning has had significant successes in computer vision thanks to the abundance of visual data, collecting sufficiently large real-world datasets for robot learning can be costly. To increase the practicality of these techniques on real robots, we propose a modular deep reinforcement learning method capable of transferring models trained in simulation to a real-world robotic task. We introduce a bottleneck between perception and control, enabling the networks to be trained independently, but then merged and fine-tuned in an end-to-end manner. On a canonical, planar visually-guided robot reaching task a fine-tuned accuracy of 1.6 pixels is achieved, a significant improvement over naive transfer (17.5 px), showing the potential for more complicated and broader applications. Our method provides a technique for more efficiently improving hand-eye coordination on a real robotic system without relying entirely on large real-world robot datasets.

## 1 Introduction

The advent of large datasets and sophisticated machine learning models, commonly referred to as deep learning, has in recent years created a trend away from hand-crafted solutions towards more data-driven ones. Learning techniques have shown significant improvements in robustness and performance [8], particularly in the computer vision field. Traditionally robotic reaching approaches have been based on crafted controllers that combine (heuristic) motion planners with the use of hand-crafted features to localize the target visually. Recently learning approaches to tackle this problem have been presented [26, 12, 1, 7]. However a consistent issue faced by most approaches is the reliance on large amounts of data to train these models. For example, Google researchers addressed this problem by developing an "arm farm" with 6-14 robots collecting data in parallel [12]. Generalization forms another challenge: many current systems are brittle when learned models are applied to robotic configurations that differ from those used in training. This leads to the question:

*Is there a better way to learn and transfer visuo-motor policies on robots for tasks such as reaching?*

Various approaches have been proposed to address these problems in a robot learning context:

- (i) the use of simulators, simulated and synthetic data [1, 4, 22];
- (ii) methods that transfer the learned models to real-world scenarios [5, 24];
- (iii) directly learning real-world tasks by collecting large amounts of data [12, 14].

In this paper, we present a method that connects these three, usually separately considered, approaches. Vision and kinematics data is gathered in simulations (cheap) to decrease the amount of real world collection necessary (costly). The approach is capable of transferring the learned models to real-world scenarios. These models can be further tuned to improved real-world performance with a fraction of the real-world data typically required for direct real-world learning approaches.

We propose a modular deep reinforcement learning approach – inspired by DQN for Atari game playing [13] – to efficiently learn and transfer visuo-motor policies from simulated to real environments, and benchmark with a visually-guided planar reaching task for a robotic arm (Figure 1). By introducing a modular approach, the perception skill and the controller can be transferred individually to a robotic platform, while retaining the ability to fine-tune them in an end-to-end fashion to further improve hand-eye coordination on a real robot (in this research a Baxter).

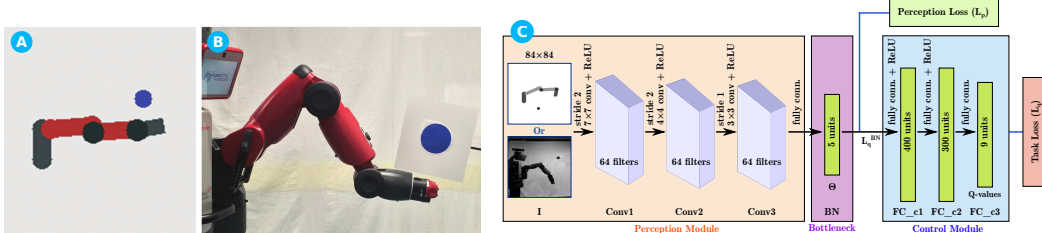


Figure 1: We present a technique for efficient learning & transfer of visuo-motor policies for reaching tasks from simulated (A) to real environments (B) using a modular deep Q network (C).

## 2 Related Work

Data-driven learning approaches have become popular in computer vision and are starting to replace hand-crafted solutions also in robotic applications. Especially robotic vision tasks – robotic tasks based directly on real image data – such as, navigation [19], object grasping and manipulation [12, 14, 10] have seen increased interest. The lack of large-scale real-world datasets, which are expensive, slow to acquire and limit the general applicability of the approach, has so far limited the broader application. Collecting the datasets required for deep learning has been sped up by using many robots operating in parallel [12]. With over 800,000 grasp attempts recorded, a deep network was trained to predict the success probability of a sequence of motions aiming at grasping on a 7 DoF robotic manipulator with a 2-finger gripper. Combined with a simple derivative-free optimization algorithm the grasping system achieved a success rate of 80%. Another example of dataset collection for grasping is the approach to self-supervised grasping learning in the real world where force sensors were used to autonomously label samples [14]. After training with 50,000 real-world trials using a staged learning method, a deep convolutional neural network (CNN) achieved a grasping success rate around 70%. These are impressive results but achieved at high cost in terms of dollars, space and time.

DeepMind showed that a deep reinforcement learning system is able to directly synthesise control actions for computer games from vision data [13]. While this result is an important and exciting breakthrough it does not transfer directly to real robots with real cameras observing real scenes [26]. In fact very modest image distortions in the simulation environment (small translations, Gaussian noise and scaling of the RGB color channels) caused the performance of the system to fall dramatically. Introducing a real camera observing the game screen was even worse [23].

There has been increasing interest to create robust visuo-motor policies for robotic applications, especially in reaching and grasping. Levine et al. introduced a CNN-based policy representation architecture with an added guided policy search (GPS) to learn visuo-motor policies (from joint angles and camera images to joint torques) [11], which allow to reduce the number of real world training by providing an oracle (or expert’s initial condition to start learning). Impressive results were achieved in complex tasks, such as hanging a coat hanger, inserting a block into a toy, and tightening a bottle cap. Recently it has been proposed to simulate depth images to learn and then transfer grasping skills to real-world robotic arms [25], yet no adaptation in the real-world has been performed.

Transfer learning attempts to develop methods to transfer knowledge between different reinforcement learning tasks [20]. To reduce the amount of data collected in the real world (expensive), transferring skills from simulation to the real world is an attractive alternative. Progressive neural networks are leveraged to improve transfer and avoiding catastrophic forgetting when learning complex sequences of tasks [15]. Their effectiveness has been validated on reinforcement learning tasks, such as Atari and 3D maze game playing. Modular reinforcement learning approaches have shown skill transfer capabilities in simulation [3]. However, methods for real-world robotic applications are still scarce and require manually designed mapping information, e.g. similarity-based approach to skill transfer for robots [5]. To reduce the number of real-world images required, a method of adapting visual representations from simulated to real environments was proposed, achieving a success rate of 79.2% in a “hook loop” task, with 10 times less real-world images [24].

### 3 Methodology

Reinforcement learning [17] has been proposed for agents to learn novel behaviours. One approach for learning from rewards is Q-learning [16], which aims to obtain a policy  $\pi$  that maximizes the expectation of accumulated rewards by approximating an optimal Q-value function

$$Q^*(s, a) = \max_{\pi} \mathbb{E} \left[ \sum_{i=0}^{\infty} \gamma^i r_{t+i} | s_t = s, a_t = a, \pi \right], \quad (1)$$

where  $r_t$  is the reward at each time step  $t$ , when following a behaviour policy  $\pi = P(a|s)$  that determines which action  $a$  to take in each state  $s$ .  $\gamma$  is a discount factor applied to future rewards. A deep neural network was introduced to approximate the Q-value function, named Deep Q Network (DQN) [13]. The state can therefore be represented by a high-dimensional raw-pixel image, since latent state features can be extracted by the convolutional layers [8]. However, learned visuo-motor policies with high-level (raw pixel) input do not transfer directly from simulated to real robots [26].

#### 3.1 Modular Deep Q Networks

Studies of deep visuo-motor policies indicate that the convolutional layers focus on perception, i.e., extracting useful information from visual inputs, while the fully connected (FC) layers perform control. To make the learning and transfer of perception and control more efficient, we propose to separate the DQN into perception and control modules connected by a bottleneck layer (Figure 1C). The **bottleneck** forces the network to learn a low-dimensional representation, not unlike Auto-encoders [6]. The difference is that we **explicitly equate** the bottleneck layer with the minimal **scene configuration**  $\Theta$  which has physical meaning. The values in  $\Theta$  are normalized to the interval  $[0, 1]$ .

With the bottleneck, the perception module learns how to estimate the scene configuration  $\hat{\Theta}$  from a raw-pixel image  $I$ ; the control module learns to approximate the optimal Q-value function as defined in Eq. 1, determining the most appropriate action  $a^*$  given the scene configuration  $\Theta$ , i.e.,  $a^* = \max_a Q(\Theta, a)$ .

#### 3.2 Training Method

The **perception network** is trained using supervised learning – first conducted in simulation, then fine-tuned with a small number of real samples for skill transfer – with the quadratic loss function

$$L_p = \frac{1}{2m} \sum_{j=1}^m \|y(I^j) - \Theta^j\|^2, \quad (2)$$

where  $y(I^j)$  is the prediction of  $\Theta^j$  for  $I^j$ ;  $m$  is the number of samples. The physical meaning of  $\Theta$  guarantees the convenience of collecting labelled training data.

The **control network** is trained using Q-learning, where weights are updated using the Bellman equation which is equivalent to the loss function

$$L_q = \frac{1}{2m} \sum_{j=1}^m \left\| Q(\Theta_t^j, a_t^j) - (r_t^j + \gamma \max_{a_{t+1}^j} Q(\Theta_{t+1}^j, a_{t+1}^j)) \right\|^2, \quad (3)$$

where  $Q(\Theta_t^j, a_t^j)$  is the Q-value function;  $\gamma$  is the discount factor applied to future rewards.

**End-to-end fine-tuning using weighted losses** Aiming for a better hand-eye coordination, an end-to-end fine-tuning is conducted for a combined network (perception + control) after their separate training, using weighted task ( $L_q$ ) and perception ( $L_p$ ) losses. The control network is updated using only  $L_q$ , while the perception network is updated using the weighted loss

$$L = \beta L_p + (1 - \beta) L_q^{BN}, \quad (4)$$

where  $L_q^{BN}$  is a pseudo-loss which reflects the loss of  $L_q$  in the bottleneck (BN);  $\beta \in [0, 1]$  is a balancing weight. From the backpropagation algorithm [9], we can infer that  $\delta_L = \beta \delta_{L_p} + (1 - \beta) \delta_{L_q^{BN}}$ , where  $\delta_L$  is the gradients resulted by  $L$ ;  $\delta_{L_p}$  and  $\delta_{L_q^{BN}}$  are the gradients resulting respectively from  $L_p$  and  $L_q^{BN}$  (equivalent to that resulting from  $L_q$  in the perception module).

## 4 Benchmark: Robotic Reaching

We use the canonical planar reaching task in [26] as a benchmark to evaluate the feasibility of the modular DQN and its training method. The task is defined as controlling a robot arm so that its end-effector position  $\mathbf{x}$  in operational space moves to the position of a target  $\mathbf{x}^* \in \mathbb{R}^m$ . The robot’s joint configuration is represented by its joint angles  $\mathbf{q} \in \mathbb{R}^n$ . The two spaces are related by the forward kinematics, i.e.,  $\mathbf{x} = \mathcal{K}(\mathbf{q})$ . The reaching controller adjusts the robot configuration to minimize the error between the robot’s current and target position, i.e.,  $\|\mathbf{x} - \mathbf{x}^*\|$ . In this task, we use the target position  $\mathbf{x}^*$  and arm configuration  $\mathbf{q}$  to represent the scene configuration  $\Theta$ . We consider a robotic arm (Figure 1) with 3 degrees of freedom (DoF), i.e.,  $\mathbf{q} \in \mathbb{R}^3$  steering its end-effector position in the plane i.e.,  $\mathbf{x} \in \mathbb{R}^2$  – ignoring orientation.

**Task Setup:** The real-world task employs a Baxter robot’s left arm (Figure 1B). to reach (in a vertical plane) for an arbitrarily placed blue target using vision. We control only three joints, keeping the others fixed. At each time step a single action of 9 possible  $a \in \mathbf{a}$  is chosen to change the robot configuration, 3 per joint: increasing or decreasing by a constant amount (0.04 rad) or leaving it unchanged. A fixed monocular camera provides raw-pixel image inputs.

**Simulator:** A simple simulator was created that, given a scene configuration  $\Theta = [\mathbf{x}^* \mathbf{q}] \in \mathbb{R}^5$ , generates the corresponding image. It creates images using a simplistic representation of a Baxter arm (in configuration  $\mathbf{q}$ ) and the target (at location  $\mathbf{x}^*$ ) represented by a blue disc with a radius of 3.8 pixels in the image (9 cm). A reach is deemed successful if the robot reaches and keeps its end-effector within 7 pixels of the target’s centre for four consecutive actions. Experimental results show that although the simulator is low-fidelity, and therefore cheap and fast for data collection, reaching skills can be learned and transferred to the real robot.

**Network Architecture:** The perception network for the task has an architecture as shown in Figure 1C, which consists of 3 convolutional and 1 fully-connected (FC) layer. Images from the simulator or the webcam (RGB, cropped to  $160 \times 210$ ) are converted to grey-scale and downsized to  $84 \times 84$  as inputs to the network. The control network consists of 3 fully-connected layers, with 400 and 300 units in the two hidden layers (Figure 1C). Input to the control network is the scene configuration  $\Theta$ , its outputs are the Q-value estimates for each of the 9 possible actions. Networks with a first convolutional layer initialized with weights from pre-trained GoogLeNet [18] (on ImageNet data [2]) were observed to converge faster and achieve higher accuracy. Note that a weight conversion, based on standard RGB to grey-scale mapping, is necessary. The other parts of the networks are initialized with random weights.

**Reward** The reward  $r$  for Q learning is determined by the Euclidean distance  $d = \|\mathbf{x} - \mathbf{x}^*\|$  between the end-effector and the target disc’s centre

$$r = \begin{cases} \lambda(\delta/d - 1), & \text{if } d > \delta \\ 0, & \text{if } d \leq \delta, n < N \\ 1, & \text{if } d \leq \delta, n \geq N \end{cases} \quad (5)$$

where  $\delta$  is a threshold for reaching a target ( $\delta = 0.05\text{m}$ );  $\lambda$  is a constant discount factor ( $\lambda = 10^{-3}$ );  $n$  represents the times of  $d$  is consecutively smaller than  $\delta$  and  $N = 4$  is a threshold that determines task completion. This reward function will yield negative rewards until getting close enough to the target. This helps to take into account temporal costs during policy search, i.e., fewer steps are better. By giving positive rewards only when  $d$  is smaller than the threshold  $\delta$  for more than  $N$  consecutive times, the reward function will guide a learner to converge to a target rather than just pass through it. This reward function proves successful for learning planar reaching, but we do not claim optimality. Designing a good reward function is an active topic in reinforcement learning.

**Guiding Q Learning with K-GPS:** In Q-learning, the  $\varepsilon$ -Greedy method is frequently used for policy search. However, our experiments show that  $\varepsilon$ -Greedy works poorly for the planar reaching task when using multiple DoF (Section 5.2). Therefore, we introduce a kinematics-based controller to guide the policy search (K-GPS), i.e., guide the learning of the operational space controller with a joint-space controller, which selects actions by

$$\arg \min_a \|a[\mathbf{q}] - \mathcal{K}^{-1}(\mathbf{x}^*)\|, \quad (6)$$

where  $a[\cdot]$  is an operator that returns an updated arm configuration when executing an action, and  $\mathcal{K}^{-1}(\cdot)$  is the inverse kinematic function. The supplementary materials show the details of the DQN algorithm with K-GPS.

## 5 Experiments and Results

Perception and control networks were first trained and evaluated independently under various conditions for the benchmark reaching task. Then comparisons were made for different combined (end-to-end) networks, such as naively combined vs fine-tuned networks. Evaluations were conducted in both simulated and real scenarios: a Baxter robot arm reaching observed by a camera.

### 5.1 Assessing Robot Perception

To understand the effect of adapting perception with real images, we trained six networks for the planar reaching task with different training data as shown in Table 1. **SIM** was trained from scratch purely in simulation; **RW** was trained from scratch using real images; **P25–100** were trained by adapting **SIM** with different percentages of real images found in the mini-batches.

1418 images were collected on the real robot together with their ground truth scene configuration for use in training and adaptation. During image collection, the robot was moved to fixed arm configurations uniformly distributed in the joint space. The target (blue disc) is rendered into the image at a random position to create a large number of training samples. Figure 2 shows a typical scene during data capture and a final dataset image after scaling, cropping and target addition. To increase the robustness of the trained network the image dataset was augmented by applying transformations to the original images (rotation, translation, noise, and brightness).

In both training and adaptation, RmsProp [21] was adopted using a mini-batch size of 128 and a learning rate between 0.1 and 0.01. The networks trained from scratch converged after 4 million update steps (~6 days on a Tesla K40 GPU). In contrast, those adapted from **SIM** converged after only 2 million update steps. Performance was evaluated using perception error, defined as the Euclidean norm between the predicted and ground truth scene configuration  $e = \|\hat{\Theta} - \Theta^*\|$ .

We compare three different scenarios:

**[Sim]** 400 simulator images, uniformly distributed in the scene configuration space

**[Real]** 400 images collected using the real robot but withheld during training

**[Live]** 40 different scene configurations during live trials on Baxter

Results with mean  $e_\mu$  and standard deviation  $e_\sigma$  of  $e$  are in in Table 1. As expected, the perception network performed well in the scenarios in which they were trained or adapted but poorly otherwise. The network trained with only simulated images (**SIM**) had a small error in simulation but very poor performance in real scenarios (Real and Live). Similarly, the network trained (**RW**) or adapted (**P100**) with only real images performed fine in real scenarios but poorly in simulation. In contrast, the networks adapted with a mixture of simulated and real images coped with all scenarios.

Results for **P25** to **P100** show that the fraction of real images in a mini-batch is important for balancing real and simulated environment performance (Figure 3). The more real images presented during training the smaller the real world experiment error became – similarly for simulation. In particular, **P25** had the smallest mean error  $e_\mu$  in simulation and **P100** the smallest  $e_\mu$  for real world and live scenarios. However, when balancing  $e_\mu$  and  $e_\sigma$ , **P75** had the best performance when tested live on Baxter: it had a smaller  $e_\sigma$  and only slightly larger  $e_\mu$  compared to **P100**.

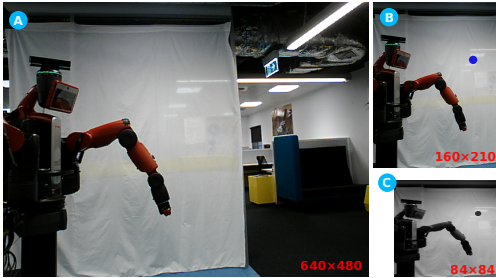


Figure 2: Images from a webcam (A) are first cropped and scaled to match the simulator size, a virtual target is also added (B). Like the simulator images, it is then converted to grey-scale and scaled to  $84 \times 84$  (C).

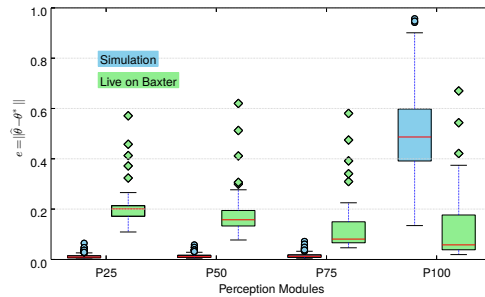


Figure 3: Distance errors for networks **P25** to **P100** in simulation (blue) and during live trials on Baxter (green). The circles and diamonds represent outliers.



Table 1: Perception Networks, Conditions and Error Reported

Nets	Training Conditions	Sim		Real		Live	
		$e_\mu$	$e_\sigma$	$e_\mu$	$e_\sigma$	$e_\mu$	$e_\sigma$
<b>SIM</b>	Train from scratch, sim images	0.013	0.009	13.92	0.877	13.53	1.436
<b>RW</b>	Train from scratch, real images	0.537	0.191	0.023	0.046	0.308	0.138
<b>P25</b>	Adapt <b>SIM</b> , 25% real, 75% sim imgs	<b>0.012</b>	0.008	0.025	0.044	0.219	0.091
<b>P50</b>	Adapt <b>SIM</b> , 50% real, 50% sim imgs	0.013	0.008	0.024	0.045	0.192	0.109
<b>P75</b>	Adapt <b>SIM</b> , 75% real, 25% sim imgs	0.015	0.010	0.021	0.046	0.135	0.123
<b>P100</b>	Adapt <b>SIM</b> , 100% real-world images	0.498	0.162	<b>0.019</b>	0.049	<b>0.133</b>	0.153

Comparing the performance in simulation we see that the network adapted with no simulated images (**P100** in Figure 3) resulted in a much larger error than **SIM**. This indicates that the presence of simulated images in adaptation prevents a network from forgetting the skills learned. We also observe that, a network adapted using only real images (**P100**) had a smaller error than one trained from scratch (**RW**). This indicates that adaptation from a pre-trained network leads to better performance as well as reduces the training time.

For all networks except **SIM** live trial results on Baxter were similar to the performance on the real world testing set, with larger errors. While the collected real world dataset was augmented with translations and rotations this indicates a high sensitivity of the perception networks to variations in camera pose (between capture of the training/testing images and the live trials). To test this indication we trained perception networks *without* data augmentation, which resulted in significantly poorer performance during live trials.

To check sensible network behaviour, we investigated the perception networks behaviour when no target was present. All trained nets output incorrect constant values (with small variance) for the target position prediction. When images with two targets were presented to the networks, a random mixture of the two target positions were output. However in both cases, joint angles were estimated accurately. When part of the robot body or arm was occluded, as shown in Figure 5, the arm configurations were still estimated well, although with a slightly greater error in most cases.

## 5.2 Assessing Robot Control

We trained 6 control networks in simulation for the planar reaching task with varying degrees of freedom using  $\epsilon$ -Greedy or K-GPS policy search. In the 1 DoF case, only  $q_2$  was active; 2 DoF uses  $q_2$  and  $q_3$ ; while 3 DoF controls all three joints. In training, we used a learning rate between 0.1 and 0.01, and a mini-batch size of 64. The  $\epsilon$  probability decreased from 1 to 0.1 within 1 million training steps for 1 DoF reaching, 2 million steps for 2 DoF, and 3 million steps for 3 DoF.  $\epsilon$ -Greedy and K-GPS used the same  $\epsilon$ .

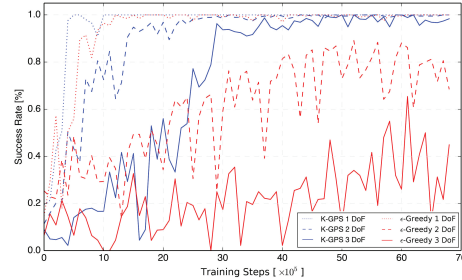


Figure 4: Learning curves showing that K-GPS converges faster than  $\epsilon$ -Greedy.

Figure 4 shows the learning curves indicating the success rate of a network after a certain number of training steps. For each data point 200 reaching tests were performed using the criteria introduced in Section 4. The target positions and initial arm configurations were uniformly distributed in the scene configuration space. For 1 DoF reaching, networks trained using K-GPS and  $\epsilon$ -Greedy both converged to a success rate of 100% after around 1 million steps (4 hrs on one 2.66GHz 64bit Intel Xeon processor core). For the 2 DoF case, K-GPS and  $\epsilon$ -Greedy converged to around 100% and 80% and took 2 million (8 hrs) and 4 million steps respectively. For 3 DoF reaching, they converged to about 100% and 40% after 4 million and 6 million (24 hrs) steps respectively. The results show that K-GPS was feasible for all degrees of freedom, while  $\epsilon$ -Greedy worked appropriately only in 1 DoF reaching and degraded as the number of DoF increased.

For a more detailed comparison, we further analyzed the error distance  $d$  – the Euclidean distance between the end-effector and target – reached by a converged network. 400 reaching tests were

Table 2: Performance of  $\varepsilon$ -Greedy and K-GPS

DoF	$d_{\text{med}}$ [cm]		$d_{Q3}$ [cm]		$\alpha$ [%]	
	$\varepsilon$ -Greedy	K-GPS	$\varepsilon$ -Greedy	K-GPS	$\varepsilon$ -Greedy	K-GPS
1	1.0	<b>0.7</b>	2.3	<b>1.1</b>	<b>100.00</b>	<b>100.00</b>
2	4.9	<b>2.8</b>	9.0	<b>3.7</b>	83.75	<b>99.50</b>
3	14.5	<b>3.4</b>	28.5	<b>4.3</b>	50.25	<b>98.50</b>

Table 3: End-to-end Reaching Performance

Scenario	Nets	$d_{\text{med}}$		$d_{Q3}$		$\bar{R}$ [ $\lambda$ ]
		[cm]	[pixels]	[cm]	[pixels]	
Sim	EE1 ( <b>SIM</b> +CR)	4.7	2.0	6.7	2.8	0.313
	EE2 ( <b>P75</b> +CR)	4.6	1.9	6.2	2.6	0.319
	<b>EE2-FT</b>	<b>3.6</b>	<b>1.5</b>	<b>4.8</b>	<b>2.0</b>	<b>0.626</b>
	CR (Control Only Baseline)	3.4	1.4	4.3	1.8	0.761
Real	EE1	41.8	17.5	80.2	33.6	-0.050
	EE2	4.6	1.9	6.2	2.6	0.219
	<b>EE2-FT</b>	<b>3.7</b>	<b>1.6</b>	<b>5.2</b>	<b>2.2</b>	<b>0.628</b>
	CR (Control Only Baseline)	3.2	1.3	4.3	1.8	0.781

performed for each network in simulation. The results are summarized in Table 2 which shows that K-GPS achieved smaller error distances for both median  $d_{\text{med}}$  and third quartile  $d_{Q3}$  than  $\varepsilon$ -Greedy.

To evaluate the performance of a control network in real scenarios, a K-GPS trained network (3 DoF) was directly transferred on Baxter. In the test, joint angles were taken from the robot’s encoders and the target position was set externally. It achieved a median distance error of 1.3 pixels (3.2 cm) in 20 consecutive reaching trials (CR in Table 3), indicating robustness to real-world sensing noise.

In addition to the proposed FC network architecture, we also tested several other control network architectures, varying the number of hidden layers and the number of units in each layer. Qualitative results show that a network with only one hidden layer was enough for 1 DoF reaching but insufficient for 2 and 3 DoF cases. The number of units in each layer also influenced the performance. Our proposed architecture worked best for 3 DoF reaching; at least two hidden layers with 200 and 150 units were needed.

### 5.3 End-to-end Network Performance

We evaluated the end-to-end performance of combined networks in both simulated and real-world scenarios using the metrics of Euclidean distance error  $d$  (between the end-effector and target) and average accumulated reward  $\bar{R}$  (a bigger accumulated reward means a faster and closer reaching to a target) in 400 simulated trials or 20 real trials. When testing in real scenarios, virtual targets were rendered into the image stream from the camera for repeatability and simplicity.

For comparison, we evaluated three networks end-to-end: EE1, EE2 and EE2-FT. EE1 is a combined network comprising **SIM** and CR; EE2 consists of **P75** and CR; EE2-FT is EE2 after end-to-end fine-tuning using weighted losses. **P75** and CR are the selected perception and control modules which have the best performance individually.

In the end-to-end fine-tuning,  $\beta = 0.8$ , we used a learning rate between 0.01 and 0.001, a mini-batch size of 64 and 256 for task and perception losses respectively, and an exploration possibility of 0.1 for K-GPS. These parameters were empirically selected. To make sure that the perception module remembers the skills for both simulated and real scenarios, the 1418 real samples were also used to obtain  $\delta_{L_p}$ . Similar to **P75**, 75% samples in a mini-batch were from real scenarios, i.e., at each weight updating step, 192 extra real samples were used in addition to the 64 simulated samples in the mini-batch for  $\delta_{L_q}$ .

The error distances in cm and pixels (in the  $84 \times 84$  image) are compared. (Table 3,  $d_{\text{med}}$  and  $d_{Q3}$  are the median and third quartile of  $d$ ). The baseline CR network, where perfect perception is assumed is added as baseline. From the results in simulation, we can see that EE1 and EE2 have similar performance in all metrics. After end-to-end fine-tuning, EE2-FT achieved a much better performance (21.7% smaller  $d_{\text{med}}$  and 96.2% bigger  $\bar{R}$ ) than EE2. The fine-tuned performance is very close to that of the control module (CR) which controls the arm using ground-truth  $\Theta$  as

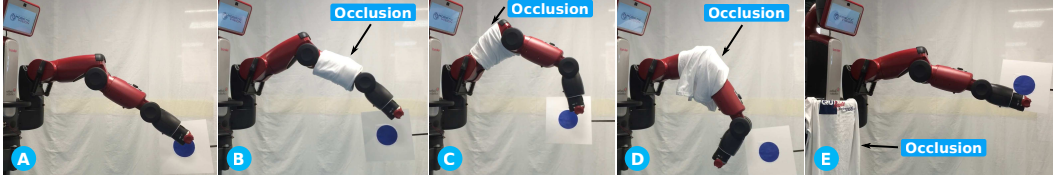


Figure 5: Successful reaching with real targets (A) and occlusions (B-E) not present during training.

sensing inputs. This indicates the proposed fine-tuning approach significantly improved the hand-eye coordination.

In the real world, as expected, EE1 worked poorly, since the perception network had not experienced real scenarios. In contrast, EE2 and EE2-FT worked well and achieved comparable performance to that in simulation. Note: that due to the cost of real world experiments, only 20 trials each were run (compared to 400 in simulation). Benefiting from the end-to-end fine-tuning, EE2-FT achieved a median distance error of 3.7 cm (1.6 pixels). This also shows that the adaptation to real scenarios can be kept by presenting (a mix of simulated and) real samples to compute the perception loss. All networks (except EE1 in the real scenario) achieved a success rate between 98% and 100%.

To see the combined networks’ robustness to a real target and occlusions, we tested EE2-FT in the setups shown in Figure 5. In the case without occlusion (A), real targets can be reached (although only virtual targets were used for training). Occlusions had not been experienced by the network during training, yet we see that in cases B, C and E, most targets can be reached but with larger distance errors (about 2 times larger than in case A). In case D, only a few targets could be reached with a yet increased error across all cases (see attached video).

## 6 Conclusion

In this research, we demonstrated reliable vision-based planar reaching on a real robot using a modular deep Q network (DQN), trained in simulation, with transference to a real robot utilizing only a small number of real world images. The proposed end-to-end fine-tuning approach using weighted losses significantly improved the hand-eye coordination of the naively combined network (EE2). Through fine-tuning, its (EE2-FT) reaching accuracy was improved by 21.7%. This work has led to the following observations:

**Value of a modular structure and end-to-end fine-tuning:** The significant performance improvement (hand-eye coordination) and relatively low real world data requirements show the feasibility of the modular structure and end-to-end fine-tuning for low-cost transfer of visuo-motor policies. Through fine-tuning with weighted losses, a combined network comprising perception and control modules trained independently can even achieve performance very close to the control network alone (indicating the performance upper-limit). Scaling the proposed techniques to more complicated tasks and networks will likely be achievable with an appropriate scene configuration representation.

**Perception adaptation:** A small number of real-world images are sufficient to adapt a pre-trained perception network from simulated to real scenarios, even with a simulator of only modest visual fidelity. The percentage of real images in a mini-batch plays a role in balancing the performance in real and simulated environments. The presence of simulated images in fine-tuning prevents a network from forgetting pre-mastered skills. The adapted perception network also has some interesting robustness properties: it can still estimate the robot configuration even in the presence of occlusions it has not directly experienced or when there is/are zero or multiple targets.

**Control training with K-GPS:** With guidance from a kinematic controller K-GPS leads to better policies (smaller error distance) in a shorter time than  $\epsilon$ -Greedy, producing a trained control network that is robust to real-world sensing noise. However K-GPS does assume that we already have some knowledge of the task to learn, i.e., a model of the task.

We believe the architecture presented here: introducing a bottleneck between perception and control, training networks independently then merging and fine-tuning, is a promising line of investigation for robotic visual servoing and manipulation tasks. In current and future work we are scaling up the complexity of the robot tasks and further characterizing the performance of this approach. Preliminary results for a 7DOF, 3D reaching task using velocity control are promising.



## Acknowledgments

This research was conducted by the Australian Research Council Centre of Excellence for Robotic Vision (project number CE140100016). Additional computational resources and services were provided by the HPC and Research Support Group at QUT.

## References

- [1] Q. Bateux, E. Marchand, J. Leitner, F. Chaumette, and P. Corke. Visual servoing from deep neural networks. In *Workshop on New Frontiers in Deep Learning for Robotic, RSS 2017*, 2017. arXiv preprint arXiv:1705.08940.
- [2] J. Deng, W. Dong, R. Socher, L.-J. Li, K. Li, and L. Fei-Fei. Imagenet: A large-scale hierarchical image database. In *IEEE Conference on Computer Vision and Pattern Recognition (CVPR)*, 2009.
- [3] C. Devin, A. Gupta, T. Darrell, P. Abbeel, and S. Levine. Learning modular neural network policies for multi-task and multi-robot transfer. *arXiv preprint arXiv:1609.07088*, 2016.
- [4] A. D’Innocente, F. M. Carlucci, M. Colosi, and B. Caputo. Bridging between computer and robot vision through data augmentation: a case study on object recognition. *arXiv preprint arXiv:1705.02139*, 2017.
- [5] T. Fitzgerald, A. Goel, and A. Thomaz. A similarity-based approach to skill transfer. In *Women in Robotics Workshop at Robotics: Science and Systems Conference (RSS)*, 2015.
- [6] G. E. Hinton and R. R. Salakhutdinov. Reducing the dimensionality of data with neural networks. *science*, 313(5786):504–507, 2006.
- [7] K. Katyal, I.-J. Wang, and P. Burli. Leveraging deep reinforcement learning for reaching robotic tasks. In *Workshop on Deep Learning for Robotic Vision at CVPR*, 2017.
- [8] A. Krizhevsky, I. Sutskever, and G. E. Hinton. Imagenet classification with deep convolutional neural networks. In *Advances in Neural Information Processing Systems (NIPS)*, pages 1097–1105, 2012.
- [9] Y. LeCun. A theoretical framework for back-propagation. In D. Touretzky, G. Hinton, and T. Sejnowski, editors, *Proceedings of the 1988 Connectionist Models Summer School*, pages 21–28, CMU, Pittsburgh, Pa, 1988. Morgan Kaufmann.
- [10] I. Lenz, R. Knepper, and A. Saxena. Deepmpc: Learning deep latent features for model predictive control. In *Robotics: Science and Systems (RSS)*, 2015.
- [11] S. Levine, C. Finn, T. Darrell, and P. Abbeel. End-to-end training of deep visuomotor policies. *Journal of Machine Learning Research*, 17(39):1–40, 2016.
- [12] S. Levine, P. P. Sampedro, A. Krizhevsky, and D. Quillen. Learning hand-eye coordination for robotic grasping with deep learning and large-scale data collection. In *International Symposium on Experimental Robotics (ISER)*, 2016.
- [13] V. Mnih, K. Kavukcuoglu, D. Silver, A. A. Rusu, J. Veness, M. G. Bellemare, A. Graves, M. Riedmiller, A. K. Fidjeland, G. Ostrovski, et al. Human-level control through deep reinforcement learning. *Nature*, 518(7540):529–533, 2015.
- [14] L. Pinto and A. Gupta. Supersizing self-supervision: Learning to grasp from 50k tries and 700 robot hours. In *IEEE International Conference on Robotics and Automation (ICRA)*, 2016.
- [15] A. A. Rusu, M. Vecerik, T. Rothörl, N. Heess, R. Pascanu, and R. Hadsell. Sim-to-real robot learning from pixels with progressive nets. *arXiv preprint arXiv:1610.04286*, 2016.
- [16] R. Sutton and A. Barto. *Reinforcement learning: An introduction*. Cambridge Univ Press, 1998. ISBN 978-0262193986.
- [17] R. Sutton and A. G. Barto. *Reinforcement learning: An introduction*. MIT Press, 1998.

- [18] C. Szegedy, W. Liu, Y. Jia, P. Sermanet, S. Reed, D. Anguelov, D. Erhan, V. Vanhoucke, and A. Rabinovich. Going deeper with convolutions. In *IEEE Conference on Computer Vision and Pattern Recognition (CVPR)*, pages 1–9, 2015.
- [19] L. Tai, S. Li, and M. Liu. A deep-network solution towards model-less obstacle avoidance. In *IEEE/RSJ International Conference on Intelligent Robots and Systems (IROS)*, 2016.
- [20] M. E. Taylor and P. Stone. Transfer learning for reinforcement learning domains: A survey. *The Journal of Machine Learning Research*, 10:1633–1685, 2009.
- [21] T. Tieleman and G. Hinton. Lecture 6.5-rmsprop: Divide the gradient by a running average of its recent magnitude. *COURSERA: Neural Networks for Machine Learning*, 4(2), 2012.
- [22] J. Tobin, R. Fong, A. Ray, J. Schneider, W. Zaremba, and P. Abbeel. Domain randomization for transferring deep neural networks from simulation to the real world. *arXiv preprint arXiv:1703.06907*, 2017.
- [23] A. W. Tow, S. Shirazi, J. Leitner, N. Sünderhauf, M. Milford, and B. Upcroft. A robustness analysis of deep q networks. In *Australasian Conference on Robotics and Automation (ACRA)*, 2016.
- [24] E. Tzeng, C. Devin, J. Hoffman, C. Finn, P. Abbeel, S. Levine, K. Saenko, and T. Darrell. Adapting deep visuomotor representations with weak pairwise constraints. In *Workshop on the Algorithmic Foundations of Robotics (WAFR)*, 2016.
- [25] U. Viereck, A. t. Pas, K. Saenko, and R. Platt. Learning a visuomotor controller for real world robotic grasping using easily simulated depth images. *arXiv preprint arXiv:1706.04652*, 2017.
- [26] F. Zhang, J. Leitner, M. Milford, B. Upcroft, and P. Corke. Towards vision-based deep reinforcement learning for robotic motion control. In *Australasian Conference on Robotics and Automation (ACRA)*, 2015.

## A Additional Materials

### A.1 Initializing the networks

As GoogLeNet has three input channels (RGB) compared to our single (gray) channel network a weight conversion, based on standard RGB to grey-scale mapping, is necessary.

In the weight initialization of Conv1, a weight conversion is necessary, since the GoogLeNet has 3 input channels (RGB). In the conversion, we use the luminosity method to convert RGB weights to grey-scale according to the equation

$$W_Y = 0.2989 * W_R + 0.5870 * W_G + 0.1140 * W_B, \quad (7)$$

where  $W_Y$  represents a converted grey-scale weight;  $W_R$ ,  $W_G$  and  $W_B$  represent weights in the channels of red, green and blue from GoogLeNet.

### A.2 Image resizing

When being input to our modular DQN, the simulator screens (and real images) are resized from  $160 \times 210$  to  $84 \times 84$ , and converted to grey-scale images.

### A.3 Details about the K-GPS algorithm

By introducing the guidance of a kinematic controller in Q learning, better policies were obtained in a shorter time. The K-GPS algorithm is shown here.

---

**Algorithm 1:** DQN with K-GPS

---

```
1 Initialize replay memory  $\mathbf{D}$ 
2 Initialize Q-function  $Q(\Theta, a)$  with random weights
3 for  $iteration=1, K$  do
4   if previous trial finished then
5     Start a new trial:
6     Randomly generate configurations  $\mathbf{q}$  and  $\mathbf{q}^*$ 
7     Compute the end-effector position  $\mathbf{x}^* = \mathcal{K}(\mathbf{q}^*)$ 
8   end
9   if  $rand(0,1) < \varepsilon$  then  $a_t = \arg \min_a \|a[\mathbf{q}] - \mathbf{q}^*\|$ 
10    else  $a_t = \arg \max_a Q(\Theta_t, a)$ 
11    Execute  $a_t$  and observe reward  $r_t$  and state  $\Theta_{t+1}$ 
12    Add the new sample  $(\Theta_t, a_t, r_t, \Theta_{t+1})$  into  $\mathbf{D}$ 
13    Sample a random mini-batch from  $\mathbf{D}$ 
14    Update  $(Q(\Theta, a))$  using the mini-batch
15 end
```

---

A replay memory  $\mathbf{D}$  is used to store samples of  $(\Theta_t, a_t, r_t, \Theta_{t+1})$ . At the beginning of each trial, the arm's starting configuration and target position are randomly generated. To guarantee a random target position  $\mathbf{x}^*$  is reachable by the arm, we first randomly select an arm configuration  $\mathbf{q}^*$ , then use the position of its end-effector as the target position.  $\mathbf{q}^*$  ( $= \mathcal{K}^{-1}(\mathbf{x}^*)$ ) is also used as the desired configuration to guide the policy search. In each iteration, the action will be selected either by the kinematic controller (with probability  $\varepsilon$ ) or by the control network. During training,  $\varepsilon$  decreases linearly from 1 to 0.1, i.e., the guidance gets weaker in the process. The newly observed sample  $(\Theta_t, a_t, r_t, \Theta_{t+1})$  is added to  $\mathbf{D}$  before the network is updated using a mini-batch randomly selected from  $\mathbf{D}$ .